Next Generation of the Albira Small Animal PET Based on SiPM Detectors and Continuous Crystals

Author: A González[1], C Correcher[2], C Molinos[2], JM Benlloch[1], S Junge[3] and T Bruckbauer[4]

[1]I3M Valencia, 46022, SPAIN, [2]Oncovision, Valencia, 46013, SPAIN, [3]Bruker BioSpin GmbH, Ettlingen, Germany, [4]Bruker BioSpin Corporation, Billerica, MA 01821 ,USA

This document presents the design and preliminary performance characterization of a compact yet powerful small animal PET based on Silicon Photomultiplier (SiPMs) photosensors and monolithic scintillators.

The system capabilities allow the accurate determination of all three spatial coordinates of the gamma photon interaction within the detector crystal. As a result, submillimetric spatial resolutions are possible with no special corrections and using the full field of View (FOV) of the system.

Two systems have been evaluated: a single ring with a 46 mm axial FOV and a triple ring with a 148 mm axial FOV. Both designs have an 80 mm transaxial FOV. The design will allow the PET detector to be located in-line with either MRI or uCT as well as supporting simultaneous PET-MR imaging.

Design and Technology

Detectors

The axial and transaxial FOVs of the three ring assembly are approximately 148 mm and 80 mm, respectively. The one ring version features the same transaxial FOV but a reduced axial FOV of 46 mm. The gap between adjacent scintillators has been reduced to only 0.5 mm, providing an almost closed octagonal scintillation volume.

Each array is made up by 144 SiPMs, arranged in 12 by 12 rows and columns, covering an active area of approximately 50×50 mm^2. A single LYSO scintillation block with a thickness of 10 mm has been coupled to each SiPM array. In contrast to previous Albira generations, the entrance surface of this scintillator is increased from 40×40 mm^2 to about 48×48 mm^2, with an exit face of 50×50 mm^2.

The increase in sampling from the previous Albira (12×12 compared to 8×8) allows for better determination of the light distribution. Thus, the known edge effect in continuous crystals is significantly reduced and the determination of the position of the impinging event greatly increased. Black paint has been applied to the entrance and lateral faces of the crystal to preserve the scintillation light distribution.

Figure 1

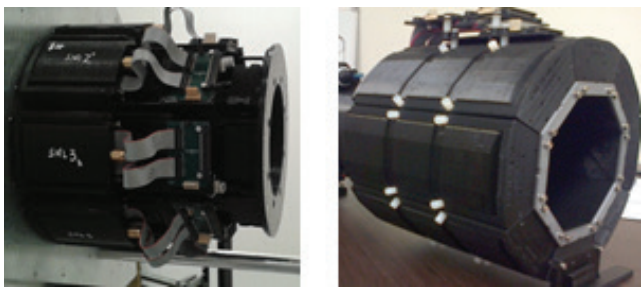

Left, one ring PET system made up by 8 detectors. Right, three ring PET system.

Figure 2

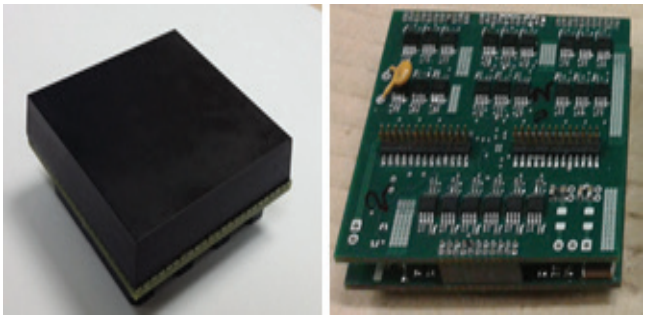

Left, assembly of monolithic LYSO scintillator and SiPM array. Right, PET module readout electronics.

Figure 3

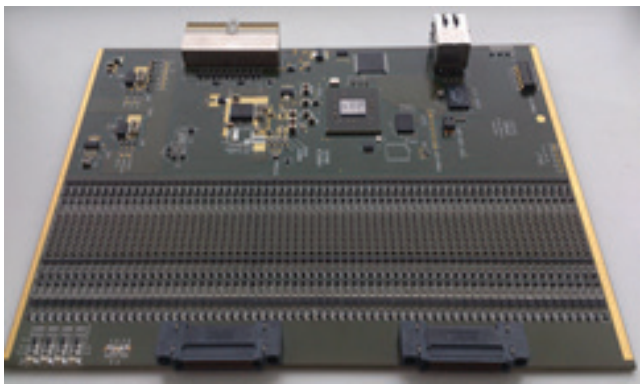

66-channel ADC board with FPGA processing capabilities. Signals are simultaneously sampled (no multiplexing). Each board digitalizes the signal from 2 PET modules. The overall DAQ system employs a 10 Gb Ethernet switch

Electronics

Each SiPM array has been directly connected to a readout circuit that provides outputs for each row and column of the array. The 24 signals, in addition to the summed trigger signal and the temperature sensor information, are transferred with flexible boards 30 cm away from the PET detector without any additional connections in between. This design avoids the use of nickel containing connectors which might interfere with the MR main field and prevents eddy currents in metallic structures that are induced by rapidly switching gradient fields of the MRI-gradient-system. The row and column signals are digitalized with custom high-speed ADC electronic boards capable of processing up to 66 channels (i.e. two detectors can be connected to one board, see Figure 3). The ADCs include FGPA processing capabilities improving the data bandwidth. A main trigger board with programmable coincidence windows (3, 5, 7 and 9 ns) starts digitization.

Figure 4

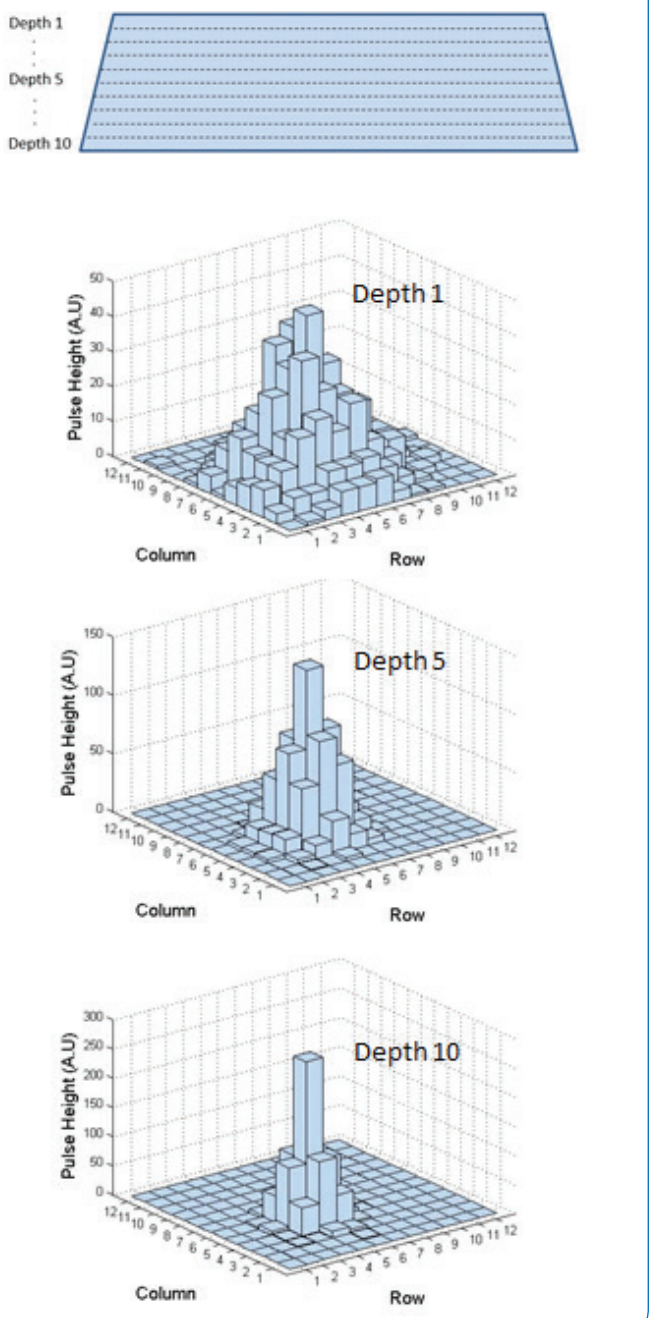

The detected light distribution becomes narrower as the gamma ray interaction occurs deeper into the scintillator crystal. The accurate measurement of the distribution and its processing allows for the DOI determination. This example shows a 10 slice sampling of the whole crystal thickness

DOI and 3D impact position

Only continuous crystals allow a full scintillation light distribution measurement and characterization. This light distribution measurement provides the key for the 3D determination of the gamma ray true point of impact. As illustrated in Figure 4, the deeper into the crystal the gamma ray interacts, the broader the light distribution will be. This effect can be used to accurately calculate the Depth of Interaction (DOI).

Each detector module provides information of both X and Y projections of the complete scintillation light distribution. As explained earlier, we have taken advantage of the knowledge of this distribution to apply a novel method to determine the 3D photon impact coordinates.

A novel approach calculates the centroid of the X and Y coordinates and the photon depth of interaction (DOI) [2]. This DOI is estimated by working out the ratio of signal sum to maximum (N/I) followed by rescaling, see figure 5. The method has shown lower compression effects than traditional centroid determination like center of gravity (CoG) or using Anger's logic.

Accurate X, Y, and DOI information, of nearly 1 mm resolution (FWHM) is obtained in all directions and used to properly calculate the true line of response, correcting for the parallax error. Figure 6 shows on the left the distribution for a small ROI corresponding to a 1 mm ^{22}Na source in a 9x9 source array. The typical behavior of exponential decay of photon impact probability with marked lower and upper limits (10 mm) can be observed. Shown on the right is the estimated DOI resolution for the 81 ROIs for the source array mentioned above, with values of about 1 mm.

Cooling

Since SiPM sensors are sensitive to bias (supply voltage) and temperature variations, all detectors are air cooled and kept at temperatures of approximately 22 °C. This effectively reduces the inherent dark noise of solid state detectors and it avoids undesired gain drifts.

The cooling system is based on compressed air allowing a quick temperature stabilization (15 minutes) yet avoiding the leak risks associated with systems based on liquid coolants.

NEMA and Non NEMA Performance Characteristics

Spatial Resolution

A NEMA point source has been used to test the spatial resolutions of the 1 ring system. We have made use of the MLEM algorithm implemented using multiple GPU with matrix voxel sizes of 0.4×0.4×0.4 mm3 and virtual pixels of 1.6×1.6 mm2.

Figure 5

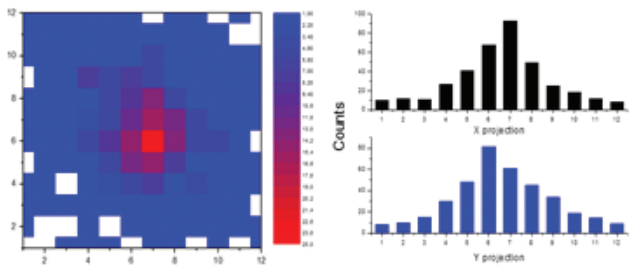

DOI is estimated with N/I (sum of signals / maximum) and then rescaled. The method has shown lower compression effects than traditional centroid determination like center of gravity (CoG).

Figure 6

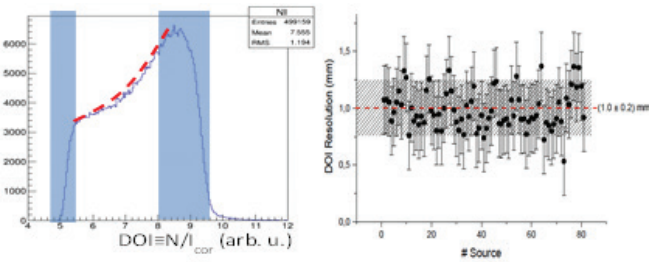

Left, measured exponential behavior of the photon interaction probability photon marked lower and upper limits (10 mm). Right, DOI resolution measurement on each of the 81 Na^{22} array sources tested.

One of the key advantages of using monolithic blocks is precisely this virtual pixilation of the scintillation crystal. See Table 1, 2 and Figure 7.

The results show an almost homogeneous spatial resolution across the entire FOV. For the expected NEMA locations, both at axial center and at ¼ of it, we have found almost identical spatial resolutions in the range of 1 to 1.2 mm for the radial, tangential and axial directions.

Figure 8 presents the volumetric resolution results with the single effect of utilizing or not the DOI (ie not accounting for the parallax error). The trend lines show the critical effect of accurately measuring the DOI.

The importance of a homogeneous spatial resolution has been debated for some time. Only consistent spatial resolution allows reproducible quantification between animal scans. Our implementation achieves constant resolution throughout almost the entire FOV. This wide field accuracy allows robustness against animal positioning variations and enhanced accuracy of results.

NEMA Sensitivity

The NEMA sensitivity has been measured on the triple ring system and a peak of approximately 9% has been reached at the center of the FOV using a 50% energy window. When using the frequently found simplification of counting all acquired events within that same energy window, the sensitivity has been found to be almost 12%.

NEMA NECR

The NEMA Noise Equivalent Count Rate has been determined both for the mouse and rat phantoms. The results show a significant improvement with respect to the current commercial system.

The mouse NECR peak has been measured at 575 kcps at an activity of 36 MBq (973 uCi). On the other hand, the rat NECR peak has been measured at 330 kcps at an activity of 47 MBq (1270 uCi). See Figures 9 and 10 for details on the count rate curves as function of the activity.

Spatial Resolution Determination Using a Derenzo-like Phantom

Point sources reconstructed with iterative algorithms can lead to an overestimation of the true spatial resolution, especially when over-iterating. For this reason and to illustrate the true resolution capabilities with animals, Derenzo-like phantom images are commonly used. See Figure 9 for the resulting image on the 1 ring system. The 0.75 mm rods are resolved showing the submillimetric capabilities. The figure shows a 120 min acquisition with 250 mCi of FDG reconstructed with MLEM using 0.25×0.25×0.25 mm^3 voxels and 1.25 mm virtual pixels. No special reconstruction corrections were applied (such as positron range estimations, PSF, Monte Carlo simulations etc). Submillimetric resolutions have also been obtained on this derenzo-like phantom on a standard 20 min acquisition followed by a less than a 30 min reconstruction on a single GPU PC. Again, no special reconstruction corrections are needed, just the standard acquisition and reconstruction settings (0.25×0.25×0.25 mm^3 voxels and 1.6 mm virtual pixels).

Table 1 Spatial Resolution at the center of FOV

(NEMA point source reconstructed with MLEM, 25 iter., 0.4 mm voxel)

	FWHM (mm)		
Radial Offset (mm)	**Radial**	**Tangential**	**Axial**
2	0,93	0,94	0,99
4	0,98	1,07	0,98
6	1,02	0,99	0,96
8	0,98	1,02	1,01
10	1,03	0,96	0,97
12	0,99	1,04	1,02
14	0,97	1,05	0,99
16	0,97	1,00	0,96
18	0,98	1,02	1,01
20	0,98	1,05	1,00
22	0,96	1,06	0,98
24	1,01	1,09	0,99
26	0,96	1,06	1,01
28	0,98	1,11	1,00
30	0,96	1,08	0,99
34	1,00	1,12	1,01
36	1,00	1,08	1,00

Figure 7

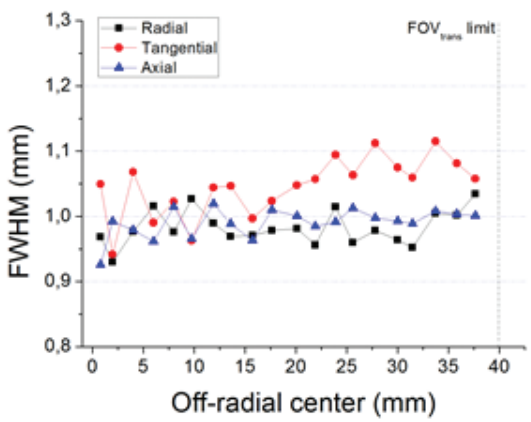

Volumetric spatial resolution at the axial center of the FOV on the single ring prototype. Effect of utilizing the DOI. MLEM reconstructions with 0.4 mm voxels and 25 iterations.

Figure 8

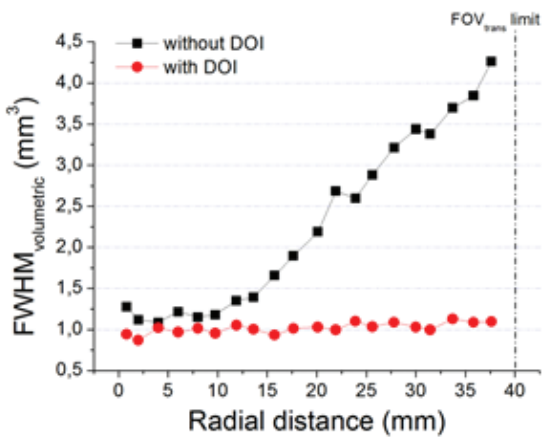

Volumetric spatial resolution at the axial center of the FOV on the single ring prototype. Effect of utilizing the DOI. MLEM reconstructions with 0.4 mm voxels and 25 iterations.

Figure 9

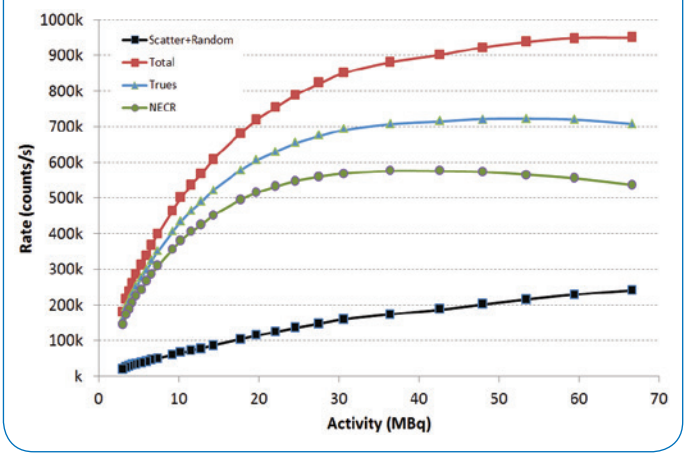

NEMA NECR performance on the mouse phantom measured on the triple ring system.

Figure 10

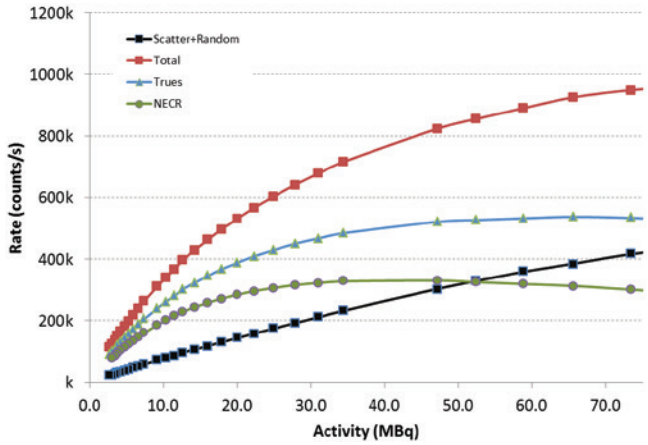

NEMA NECR performance on the rat phantom measured on the triple ring system.

In-vivo Imaging with Mice and Rats

In-vivo experiments have been carried out to evaluate the practical performance of the single ring PET. One experiment involved imaging mice and rats with NaF-18 and was carried out at the Centro de Investigación Príncipe Felipe in Valencia, Spain. Figure 12 shows a sample image of a mouse injected with 250 uCi and scanned for 15 min 1 hour post-injection. The image was reconstructed with MLEM using 25 iterations and 0.4 mm cubic voxels. The individual vertebrae and the rib cage is visualized, this high spatial resolution is consistent with the Derenzo-type images presented earlier and shows the great potential of accurate DOI correction.

A highly compact and powerful small animal PET based on Silicon Photomultiplier photosensors and monolithic scintillators has been presented.

The new system significantly outperforms the current small animal Albira PET in all tested NEMA specifications.

The system is capable of accurately determining all three spatial coordinates of the gamma impacts within the detector crystal. This allows:

- A nearly homogeneous spatial resolution for all components of 1.0 mm on average, across the entire FOV
- A submillimetric volumetric resolution with the standard default configuration for imaging small animals (15 min acquisitions and fast reconstructions)

The flexible design allows the PET detector rings to be located in-line with either MRI or uCT as well as supporting simultaneous PET-MR imaging.

References

1. NEMA, Performance Measurements of Small Animal Positron Emission, NEMA Standard Publication NU 4-2008, 2008.
2. P. Conde, et al., 3-D Photon Impact Determination Using Fitting Approaches to the Light Distribution, IEEE MIC Conf. Rec. 2014.
3. A. Goertzen, et al., NEMA NU 4-2008 Comparison of Preclinical PET Imaging Systems, J. Nucl. Med. 53, 1300-1309, 2012.

Figure 11

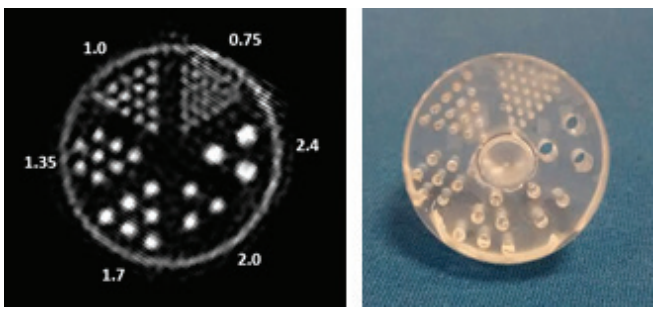

Derenzo phantom imaged with the 1 ring system. The 0.75 mm capillaries are resolved showing the submillimetric capabilities of the system. No special reconstruction corrections are needed to demonstrate submillimetric resolution.

Figure 12

NaF-18 image of a mouse. Three bed position were acquired to cover the whole body with the single ring PET

Bruker BioSpin

info@bruker.com
www.bruker.com